S1 PM_{coarse} speciation data quality

The quality of the speciation data is evaluated by examining the consistency between species concentrations obtained by different analytical methods. The evaluation is conducted for each PM size group. Deming regression is applied in the examination using the Scatter Plot computer program developed by Wu available at https://doi.org/10.5281/zenodo.832417 (Wu and Yu, 2018). The results are given in Fig. S1. Sulfate measured by IC and total S by ED-XRF exhibit an excellent consistency (R^2 = 0.99) in PM_{10} and $PM_{2.5}$ samples (Fig. S1a and b). Apart from validating the chemical analyses, the result also validates the performance of the four samplers given the sulfate and total S in PM_{10} and $PM_{2.5}$ were measured on four separate filters. The result for PM_{coarse} is scattered (Fig. S1c) because the quantification is derived from the difference between two close values as both species mostly exist in $PM_{2.5}$. Comparison between K^+ and K shows similar results (Fig. S1d–f). Cl^- and total Cl, which predominantly exist in the coarse mode, exhibit high consistency in PM_{coarse}, with R^2 of 0.91 (Fig. S1i). The cation and anion equivalence are highly consistent in PM_{10} and $PM_{2.5}$, displaying slope and R^2 values close to 1 (Fig. S1j–k). The cation equivalence appears to exceed anion for PM_{coarse} as shown in Fig. S1l, plausibly because carbonate was not measured.

The gravimetric mass is consistent with the PM data obtained from continuous monitoring by automated analyzers (oscillating microbalance/beta attenuation) at the same site, with slope and R^2 values being 1.08–1.21 and 0.95–0.98, respectively (Fig. S2a–c). The sum of chemical species strongly correlates with and is lower than the gravimetric mass (Fig. S2d–f). The difference is attributed to unmeasured ions, metal oxides, and non-carbon constituents in organic compounds. PM mass is reconstructed as the sum of geological material, organics, EC, NH_4^+, SO_4^{2-}, NO_3^-, Na^+, Mg^{2+}, Cl^-, and non-crustal elements. The geological material is estimated by multiplying coefficients accounting for oxide in the crustal elements, i.e., 1.89×[Al] + 2.14×[Si] + 1.2×[K] + 1.4×[Ca] + 1.67×[Ti] + 1.43×[Fe]. Coarse mode K is considered as a component in geological material given its strongly association with Si (R^2 = 0.98). The organic mass in $PM_{2.5}$ is approximated to be 1.6×[OC] assuming organic composition in typical urban atmosphere while that in PM_{coarse} is 2.0×[OC] considering coarse mode organics are typically associated with biological particles (Turpin and Lim, 2001). The reconstructed mass is in good agreement with the gravimetric mass for $PM_{2.5}$, with slope and R^2 values of 0.90 and 0.99, respectively (Fig. S2h). The reconstructed PM_{coarse}, however, is notably lower than the gravimetric mass, showing a slope value of 0.74 and R^2 of 0.96 (Fig. S2i). The underestimation is plausibly due to omission of constituents in geological material (e.g., carbonate) and/or water bound on PM.

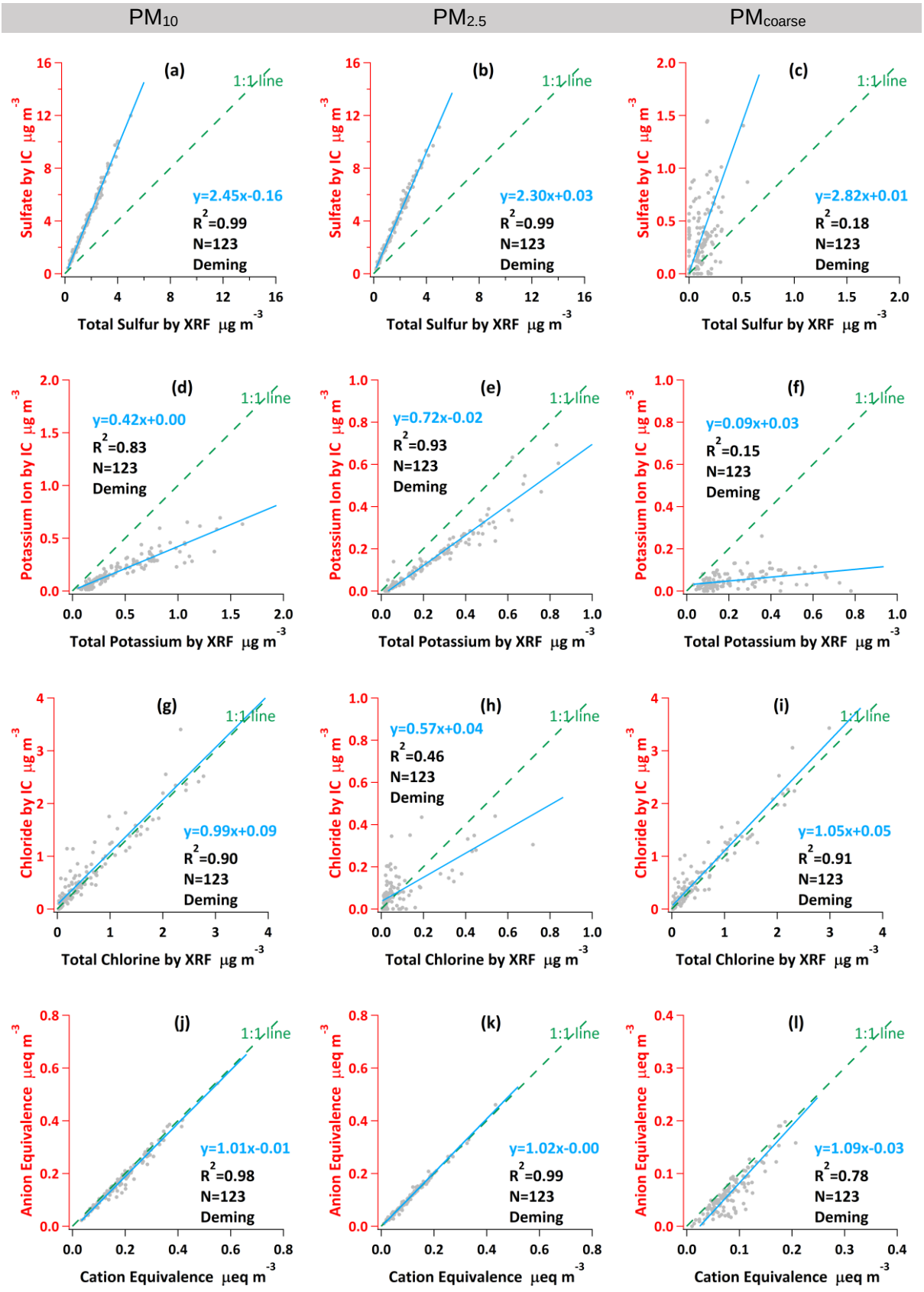

Figure S1. Evaluation of speciation data quality for PM_{10}, $PM_{2.5}$, and PM_{coarse} shown by comparison between (a–c) sulfate vs. total sulfur, (d–f) potassium ion vs. total potassium, (g–i) chloride vs. total chlorine, and (j–l) anion vs. cation equivalence.

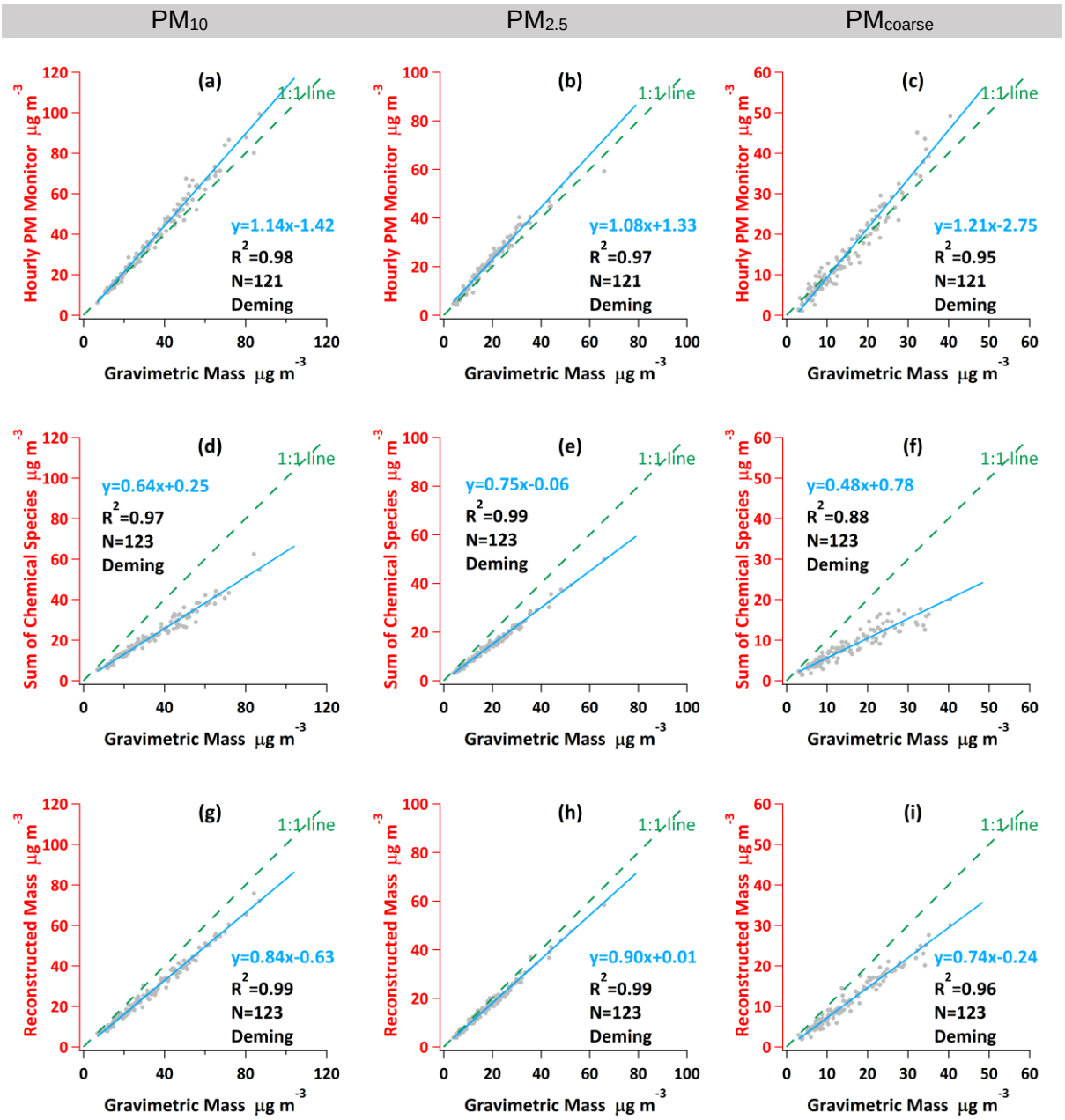

Figure S2. Evaluation of speciation data quality for PM_{10}, $PM_{2.5}$, and PM_{coarse} shown by comparison between (a–c) PM mass concentration obtained by continuous monitoring vs. gravimetric measurement, (d–f) sum of chemical species vs. gravimetric mass, and (g–i) reconstructed mass vs. gravimetric mass.

S2 Season division

Hong Kong is situated in the sub-tropical region along the southeast coast of China. The seasonal evolution of weather in Hong Kong is closely related to the East Asian Monsoon system. Therefore, the direction of upper-level wind is a reliable indicator for seasonal change around Hong Kong. Figure S3 shows the wind direction at ~20 km above ground level from December 2019 to February 2021, measured over the Hong Kong Observatory automatic weather station. It shows that the wind direction is mainly westerly in winter (December to February) and becomes easterly in summer (June to September). The transition seasons – spring and fall – are marked by a group of variable wind directions with relatively shorter duration compared to summer and winter. Four seasons can, therefore, be identified approximately.

The exact dates of the seasonal divisions are located by identifying the arrival date of the first synoptic event that is typical in the respective season; for example, cold surge in winter and arrival of warm and humid air mass in spring. These synoptic events are identified by observing the sea level pressure and dew point changes. For example, the sudden and rapid drop in sea level pressure and rise in dew point during 5–9 March 2020 indicates the arrival of warm air mass, marking the end of winter and beginning of spring. The same indicator is also used to locate the transition from spring to summer, while the opposite is used to identify the transition from summer to fall and fall to winter. The seasonal division in this study is summarized as follow:

First Winter:	1 January–9 March 2020
Spring:	10 March–17 May 2020
Summer:	18 May–7 October 2020
Fall:	8 October–28 November 2020
Second Winter:	29 November 2020–28 February 2021

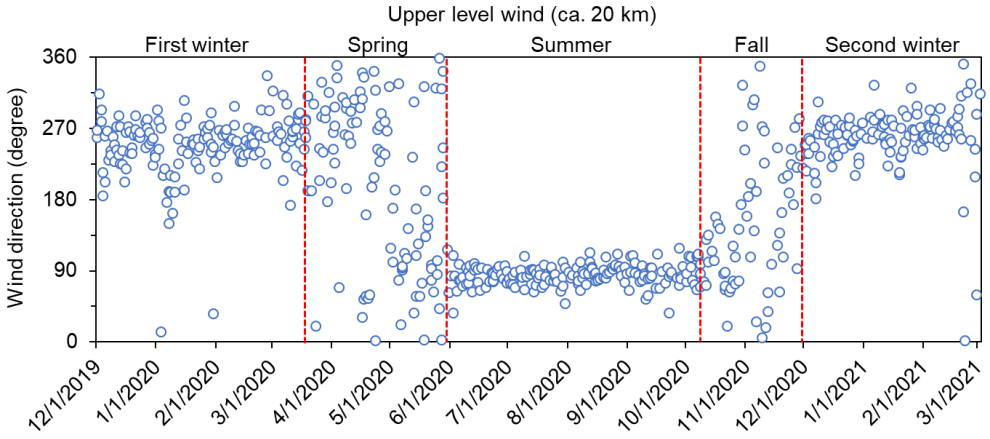

Figure S3. Temporal variation in wind direction at ~20 km height in Hong Kong during the study period.

S3 Source number determination in PMF

At first the optimal number of source factor was deduced by examining the $Q/Q_{expected}$ value for a range of PMF solutions with different factor numbers. The $Q/Q_{expected}$ value is indicative of the overall fitting of all input species and is inversely related to the fitting (Norris et al., 2014). Mathematically, the optimal factor number is the number upon which further increasing the factor number would result in much less significant improvement in the fitting, or equivalently much less reduction in $Q/Q_{expected}$ value. Figure S4 presents the $Q/Q_{expected}$ values and their changes as a function of factor number from two to eight. From the figure the three-factor solution appears to be the optimal solution since further increasing the factor number to four led to much less reduction in $Q/Q_{expected}$ value. However, we found that an additional factor is required to better reproduce the Cu concentration. Specifically, the slope and R^2 values for modeled vs. measured Cu improve from 0.54 to 0.72 and from 0.39 to 0.56, respectively, in the four-factor solution. The fourth factor is a dust-like factor enriched in Cu (Fig. 2 in main text). Considering Cu is an important species in PM health effects associated with reactive oxygen species formation, this factor is retained for source interpretation (Bates et al., 2019).

Five-factor solution was also assessed. However, the fifth factor, which is a secondary nitrate factor, was assessed to be chemically inexplainable after examining the charge balance of the ionic composition. Specifically, the factor composition is significantly depleted in cation to counterbalance nitrate (cation-to-anion equivalence ratio = 0.3). By contrast, the nitrate mainly exists in a sea salt factor in the four-factor solution, with a much more reasonable cation-to-anion equivalence ratio (1.2). This is also consistent with a previous study showing coarse nitrate in Hong Kong is mainly associated with sea salt (Bian et al., 2014). Taken all the analyses together, the four-factor solution is considered the optimal solution for source interpretation and analysis.

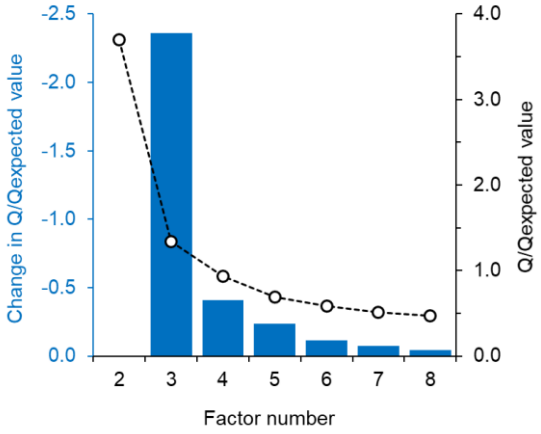

Figure S4. $Q/Q_{expected}$ values in PMF solutions of different factor numbers. The columns indicate the change in the $Q/Q_{expected}$ values as the factor number increases by one (left axis) while the circle markers indicate the $Q/Q_{expected}$ values in the solutions with corresponding factor numbers (right axis).

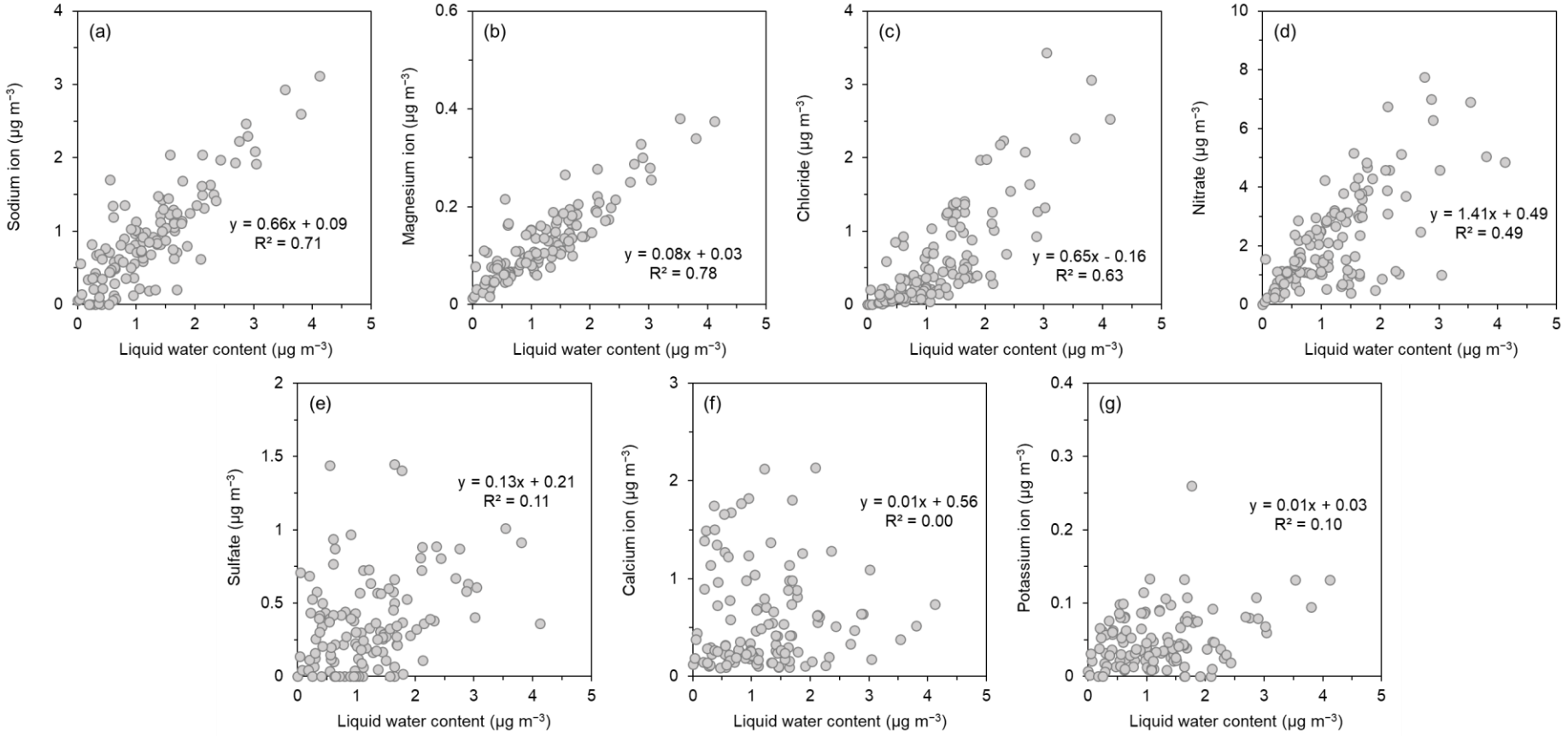

Figure S5. Correlation between aerosol liquid water content derived from ISORROPIA II thermodynamic equilibrium model and individual ionic species (*y*-axis).

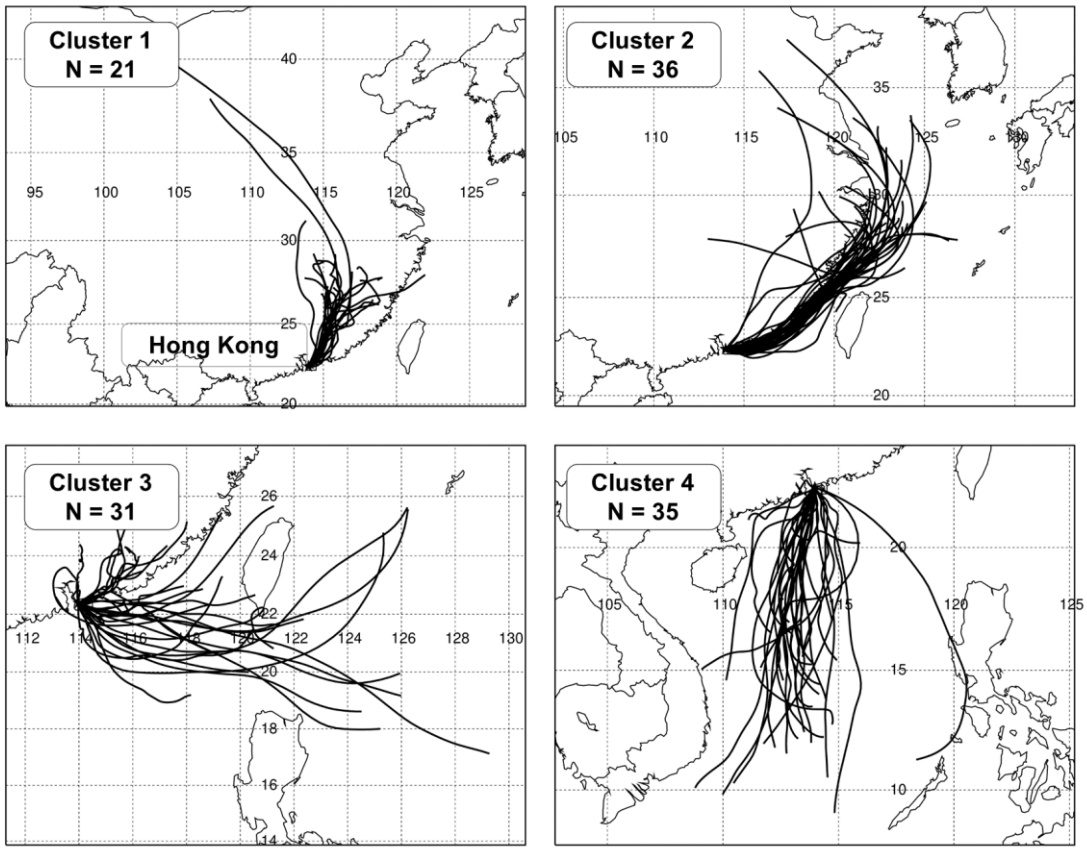

Figure S6. Individual past 48-hour backward air mass trajectories in Cluster 1 to 4 as shown in Fig. 4 in the main text.

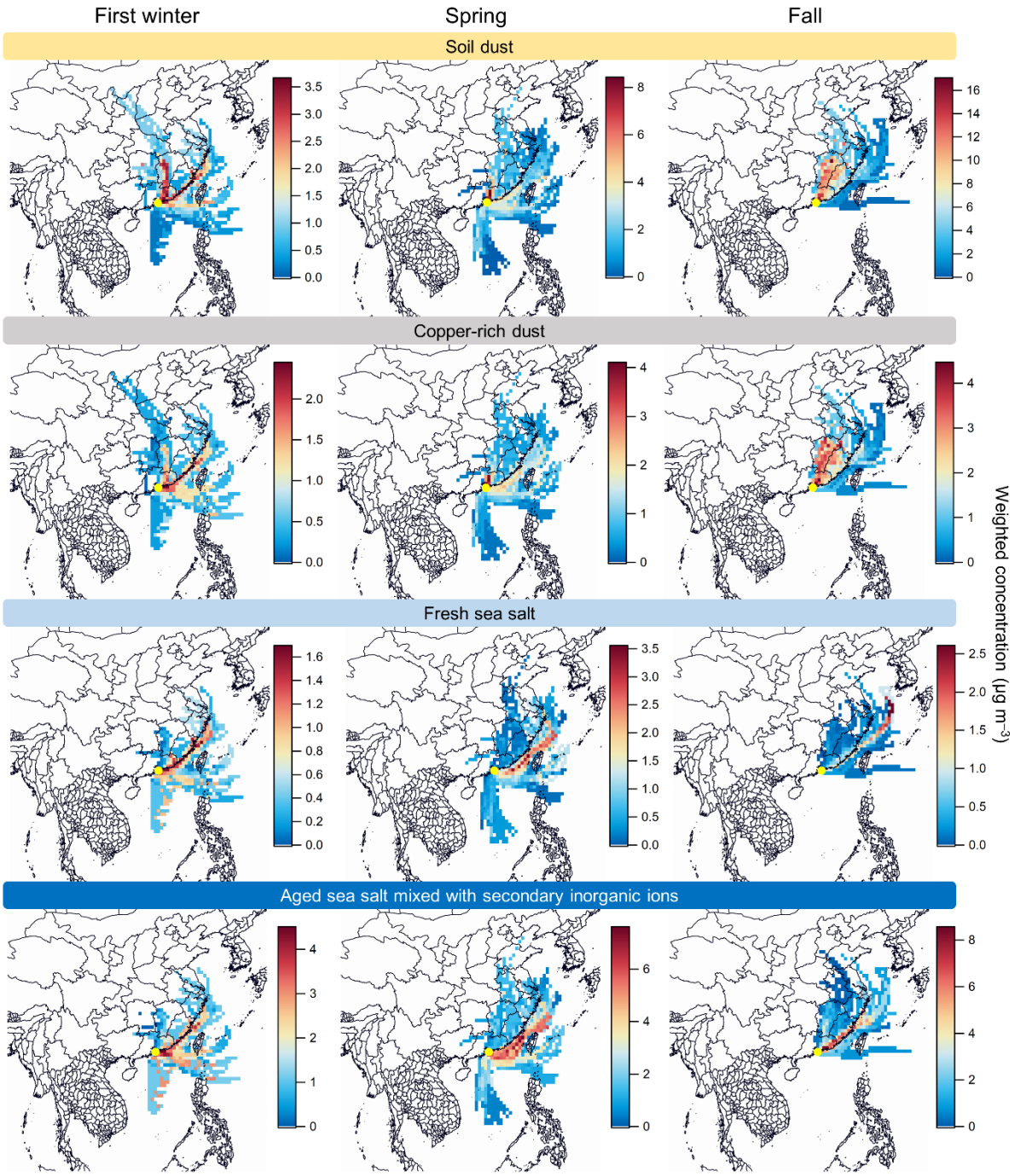

Figure S7. Concentration-Weighted Trajectory results for individual PM_{coarse} contributing sources in first winter, spring, and fall. The results for summer and second winter are shown in Fig. 5 in the main text.

Table S1. Slope, intercept, and R^2 values of PMF-modeled versus measured concentration of individual fitting species (the values for PMF without PM_{coarse} as total variable are shown in parentheses)

Species	Slope	Intercept	R^2
PM_{coarse}	1.04	-0.57	0.98
Na^+	1.01 (1.01)	-0.03 (-0.03)	0.95 (0.95)
NH_4^+	0.01 (0.01)	0.02 (0.02)	0.02 (0.02)
Mg^{2+}	0.98 (0.98)	0.00 (0.00)	0.96 (0.96)
Cl^-	0.98 (0.98)	0.01 (0.01)	1.00 (1.00)
NO_3^-	0.79 (0.79)	0.32 (0.31)	0.90 (0.90)
SO_4^{2-}	0.06 (0.06)	0.05 (0.05)	0.16 (0.16)
OC	0.30 (0.30)	0.17 (0.17)	0.44 (0.44)
EC	0.45 (0.45)	0.04 (0.04)	0.44 (0.44)
Al	0.97 (0.98)	0.01 (0.01)	1.00 (1.00)
Si	0.99 (0.99)	0.01 (0.01)	1.00 (1.00)
K	1.06 (1.07)	-0.01 (-0.01)	0.99 (0.99)
Ca	0.98 (0.98)	0.01 (0.01)	0.99 (0.99)
Ti	0.97 (0.97)	0.00 (0.00)	0.98 (0.98)
V	0.10 (0.10)	0.00 (0.00)	0.08 (0.08)
Mn	0.89 (0.89)	0.00 (0.00)	0.80 (0.80)
Fe	1.01 (1.01)	-0.01 (-0.01)	0.96 (0.96)
Ni	0.16 (0.16)	0.00 (0.00)	0.22 (0.22)
Cu	0.72 (0.72)	0.00 (0.00)	0.56 (0.55)
Zn	0.72 (0.72)	0.00 (0.00)	0.77 (0.77)
Pb	0.17 (0.17)	0.00 (0.00)	0.24 (0.24)

Table S2. Summary of the results from PMF bootstrap and displacement analyses in this study

Displacement diagnostics					
Error code:		0			
Largest decrease in Q:		0			
% dQ:		0			
Swaps by factor:		0	0	0	0
Bootstrap mapping					
	Factor 1 (Cu-rich dust)	Factor 2 (Fresh sea salt)	Factor 3 (Soil dust)	Factor 4 (Aged sea salt)	Unmapped
Boot factor 1	90	0	8	2	0
Boot factor 2	0	100	0	0	0
Boot factor 3	0	0	100	0	0
Boot factor 4	0	0	0	100	0

References

Bates, J. T., Fang, T., Verma, V., Zeng, L. H., Weber, R. J., Tolbert, P. E., Abrams, J. Y., Sarnat, S. E., Klein, M., Mulholland, J. A., and Russell, A. G.: Review of acellular assays of ambient particulate matter oxidative potential: Methods and relationships with composition, sources, and health effects, Environ. Sci. Technol., 53, 4003–4019, https://doi.org/10.1021/acs.est.8b03430, 2019.

Bian, Q. J., Huang, X. H. H., and Yu, J. Z.: One-year observations of size distribution characteristics of major aerosol constituents at a coastal receptor site in Hong Kong – Part 1: Inorganic ions and oxalate, Atmos. Chem. Phys., 14, 9013–9027, https://doi.org/10.5194/acp-14-9013-2014, 2014.

Norris, G., Duvall, R., Brown, S., and Bai, S.: EPA Positive Matrix Factorization (PMF) 5.0 fundamentals and user guide, prepared for the U. S. Environmental Protection Agency, Office of Research and Development, Washington, DC, https://www.epa.gov/sites/default/files/2015-02/documents/pmf_5.0_user_guide.pdf, 2014.

Turpin, B. J. and Lim, H. J.: Species contributions to $PM_{2.5}$ mass concentrations: Revisiting common assumptions for estimating organic mass, Aerosol Sci. Technol., 35, 602–610, https://doi.org/10.1080/02786820119445, 2001.

Wu, C. and Yu, J. Z.: Evaluation of linear regression techniques for atmospheric applications: The importance of appropriate weighting, Atmos. Meas. Tech., 11, 1233–1250, https://doi.org/10.5194/amt-11-1233-2018, 2018.